Effect of the Si/TiO$_2$/BiVO$_4$ Heterojunction on the Onset Potential of Photocurrents for Solar Water Oxidation

Hyejin Jung,[†,‡] Sang Youn Chae,[†,§] Changhwan Shin,[∥] Byoung Koun Min,[†,‡] Oh-Shim Joo,[†] and Yun Jeong Hwang*[,†,‡]

[†]Clean Energy Research Center, Korea Institute of Science and Technology, Seoul 136-791, Republic of Korea
[‡]Korea University of Science and Technology, Daejeon 305-350, Republic of Korea
[§]Department of Chemistry, College of Science, Korea University, Seoul 136-713, Republic of Korea
[∥]School of Electrical and Computer Engineering, University of Seoul, Seoul 130-743, Republic of Korea

S *Supporting Information*

ABSTRACT: BiVO$_4$ has been formed into heterojunctions with other metal oxide semiconductors to increase the efficiency for solar water oxidation. Here, we suggest that heterojunction photoanodes of Si and BiVO$_4$ can also increase the efficiency of charge separation and reduce the onset potential of the photocurrent by utilizing the high conduction band edge potential of Si in a dual-absorber system. We found that a thin TiO$_2$ interlayer is required in this structure to realize the suggested photocurrent density enhancement and shifts in onset potential. Si/TiO$_2$/BiVO$_4$ photoanodes showed 1.0 mA/cm^2 at 1.23 V versus the reversible hydrogen electrode (RHE) with 0.11 V (vs RHE) of onset potential, which were a 3.3-fold photocurrent density enhancement and a negative shift in onset potential of 300 mV compared to the performance of FTO/BiVO$_4$ photoanodes.

KEYWORDS: BiVO$_4$, Si, heterojunction, TiO$_2$, dual absorber, onset potential
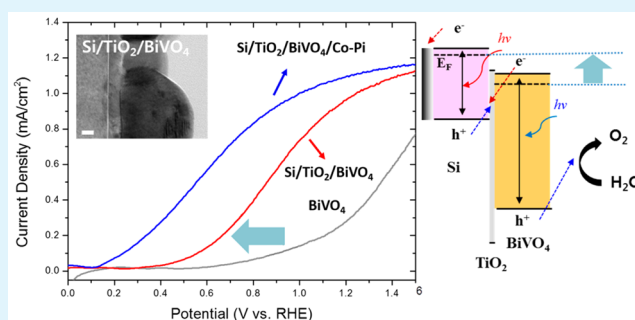
1. INTRODUCTION

In recent decades, photoelectrochemical (PEC) water splitting has been highlighted as an approach to the development of renewable energy resources,[1−3] because PEC cells can convert solar energy to chemical energy and store it in the form of hydrogen, a promising future fuel. In a PEC cell, semiconductor photoelectrodes absorb light and generate excited charge carriers (electrons and holes) to accomplish thermodynamically uphill reactions. Therefore, the development of photocatalytic semiconductor materials is critical to the achievement of high-conversion efficiency of solar power to fuel. Various metal oxide semiconductors, such as TiO$_2$, WO$_3$, Fe$_2$O$_3$, and BiVO$_4$, have been studied for water splitting applications,[4−7] because oxide materials have shown excellent stability compared to that of nitrides[8] or sulfides[9] when used as photoanodes.

Significant progress has been made with BiVO$_4$ as one of the most attractive photoanode candidates[10−12] because of its visible light absorption capability (E_g = 2.4−2.5 eV) and relatively high conduction band (CB) edge position. In the case of typical metal oxides, O 2p orbitals dominate the composition of the valence band (VB), located around 3.0 V versus a reversible hydrogen electrode (RHE), which leads to a significant energy loss. Furthermore, the CB edges of metal oxides are mainly composed of the transition metal's d orbitals. Therefore, when their band gaps are decreased to the region of

visible light, their CB edges move toward a level lower than the hydrogen reduction potential. Unlike other metal oxides, the VB of monoclinic BiVO$_4$ is composed of both O 2p and Bi 6s orbitals, which can both boost the VB edge to around 2.4 V versus RHE and maintain the CB edge level close to the hydrogen reduction potential.

Recently, photocurrent densities of BiVO$_4$ photoanodes have increased from tens of μA/cm^2 in early stages[13] to >3 mA/cm^2 through strategies such as doping,[11,14] nanomaterial synthesis,[15] and heterojunction formation.[16] In addition, the overpotential for water oxidation was significantly reduced on the surface of BiVO$_4$ with the loading of oxygen evolution reaction (OER) cocatalysts such as Co-Pi,[17] FeOOH,[18] and NiOOH.[7] However, BiVO$_4$ still requires an external bias potential for the overall water splitting in two-electrode PEC cells, which decreases the conversion efficiency of solar energy to hydrogen. For example, our previous work[15] demonstrated that a WO$_3$/BiVO$_4$ heterojunction structure could enhance the photocurrent density to 3.3 mA/cm^2 at 1.23 V versus RHE, but no photocurrent was obtained until a potential of 0.5 V versus the counter electrode (Pt) was applied, which implies that more

Scheme 1. Diagram of Charge Flows with (a) a Si/TiO$_2$/BiVO$_4$ Photoanode and (b) a WO$_3$/BiVO$_4$ Photoanode, Showing the Different Charge Separation Processes Depending on the Relative CB Potentials in the Heterojunctions
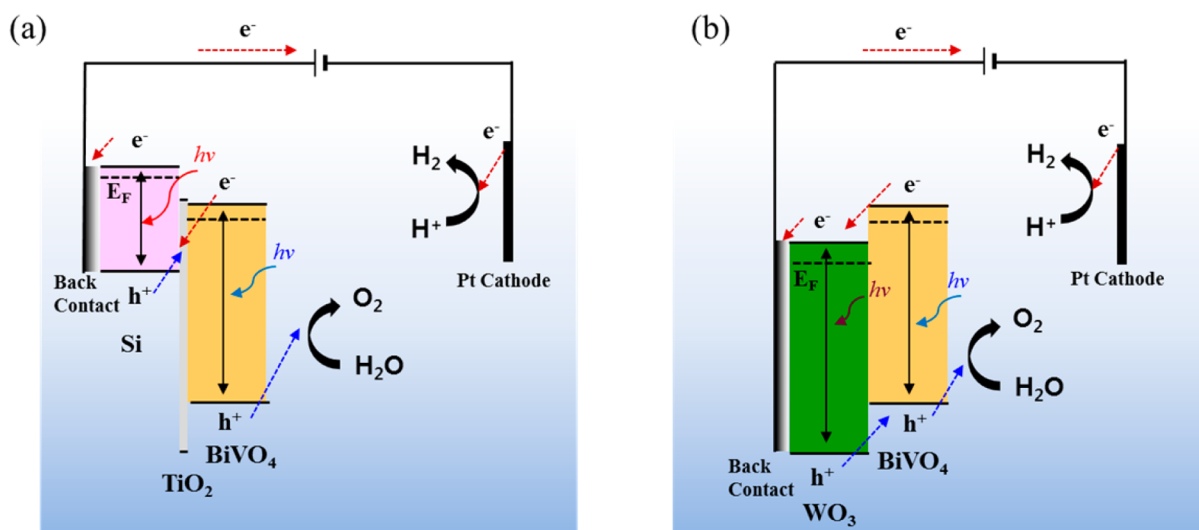
than 0.5 V of external bias potential was required to initiate overall water splitting. Therefore, the development of strategies to shift the onset potentials of the photocurrent toward the cathodic potential is as important as that to increase the photocurrent density to achieve highly efficient PEC systems with BiVO$_4$-based photoanodes.

In PEC cells, n/n heterojunction photoanodes composed of two n-type semiconductors, such as n-Si/n-TiO$_2$[19] or n-Si/n-Fe$_2$O$_3$,[20,21] have been demonstrated to increase the photocurrent density and to shift the onset potential of the photocurrent as a type of dual-absorber system. The more negative CB edge potential of Si, compared to that of TiO$_2$ or Fe$_2$O$_3$, can give higher energetics for the reduction of electrons on the counter electrode, and the charge separation efficiency can be enhanced in the metal oxide semiconductor. The photovoltages of these n/n heterojunctions are increased by the photovoltage generated at the semiconductor interface under illumination, which can contribute to the cathodic shift of the onset potential. This enhanced photoanodic activity is expected with n-Si and BiVO$_4$ heterojunctions, as well, but this behavior has not yet been observed.

Here, we demonstrate that the photoanodic performance of BiVO$_4$ can be improved by combining it with n-Si. To protect the Si surface from oxidation,[22] a thin layer of TiO$_2$ was introduced between the Si and BiVO$_4$ layers, and the influence of the interfacial TiO$_2$ thickness on the photoanodic performance was studied. Previously, BiVO$_4$ has been combined with various metal oxides to form WO$_3$/BiVO$_4$,[23,24] ZnO/BiVO$_4$,[25] and TiO$_2$/BiVO$_4$[26] heterojunctions, in which improved photocurrent density was achieved as a consequence of the facile electron transfer from the CB of BiVO$_4$ to the CB of the other metal oxides. For the electron transfer from BiVO$_4$ to the other semiconductor, the Fermi levels of WO$_3$, ZnO, or TiO$_2$ are more positive than that of BiVO$_4$ (Scheme 1), but the positive Fermi level of WO$_3$ is inferior for spontaneous water splitting applications because the thermodynamic limit of the onset potential is shifted anodically in these heterojunctions, which requires more bias potential. However, a different charge separation mechanism through carrier recombination (Scheme 1a) is suggested in the Si/TiO$_2$/BiVO$_4$ heterojunction because of the more negative CB potential of n-Si. As a dual-light

absorber system, both Si and BiVO$_4$ absorb the illuminated light to generate electrons and holes in respective layers. Scheme 1a suggests that photogenerated holes in Si and electrons in BiVO$_4$ are recombined; holes in BiVO$_4$ are used for water oxidation, while electrons in the Si layer are transferred to the counter electrode through the circuit for hydrogen evolution. With Si/TiO$_2$/BiVO$_4$ photoanodes, we demonstrate that they can decrease the onset potential of the photocurrent and increase the charge separation efficiency.

2. EXPERIMENTAL SECTION

2.1. Photoanode Preparation. n-Si(100) (phosphorus-doped, 0.3−0.6 Ω cm) and fluoride-doped tin oxide (FTO) glass (8 Ω, Pilkington) were cleaned in a 1:1 (v/v) mixture of 2-propanol and acetone by sonication for 10 min and rinsed with deionized (DI) water. To deposit a thin film of TiO$_2$ by atomic layer deposition (ALD) (Forall company), the cleaned Si and FTO substrates were placed on the hot plate of the ALD chamber, at 250 °C. Titanium(IV) isopropoxide (TTIP) (Sigma-Aldrich, 99.999%) and DI H$_2$O were used as precursors for Ti and O, respectively. A container of TTIP was heated at 50 °C. The precursor molecules were alternately introduced to the reaction chamber with Ar as a carrier gas, and an Ar purge was applied between each chemical pulse. The thickness of the TiO$_2$ thin film was controlled by varying the number of chemical pulse cycles (35, 105, 525, or 1050 cycles). BiVO$_4$ was deposited on various substrates (bare Si, TiO$_2$-deposited Si, bare FTO, and TiO$_2$-deposited FTO) following the same metal−organic decomposition method. The metal−organic precursor solution was prepared by dissolving 0.865 g of Bi(NO$_3$)$_3$·5H$_2$O (≥98%, Sigma-Aldrich) and 0.475 g of vanadyl acetylacetonate [VO(acac)$_2$] (98%, Sigma-Aldrich) in 25 mL of a 1:7.33 (v/v) solvent mixture of CH$_3$COOH (acetic acid) (≥99.7%, Sigma-Aldrich) and C$_5$H$_8$O$_2$ (acetylacetone) (≥99%, Sigma-Aldrich). The precursor solution was spin-coated at 2000 rpm for 30 s, followed by thermal treatment on a hot plate at 500 °C for 10 min. This spin-coating and thermal treatment cycle was repeated six times. A cobalt phosphate (Co-P$_i$) catalyst was loaded on the BiVO$_4$ layer by a modified previously published method.[27] An electrodeposition method was applied in a buffer solution of 0.5 mM CoCl$_2$·6H$_2$O (98%, Sigma-Aldrich) and 0.1 M potassium phosphate (pH 7.0) with an applied potential of 1.1 V versus Ag/AgCl. The deposition time was set at 2 and 4 min for Si/TiO$_2$/BiVO$_4$ and FTO/BiVO$_4$ photoanodes, respectively.

2.2. Photoelectrochemical Measurement. Photocurrents and photovoltages of the prepared photoanode samples were measured by
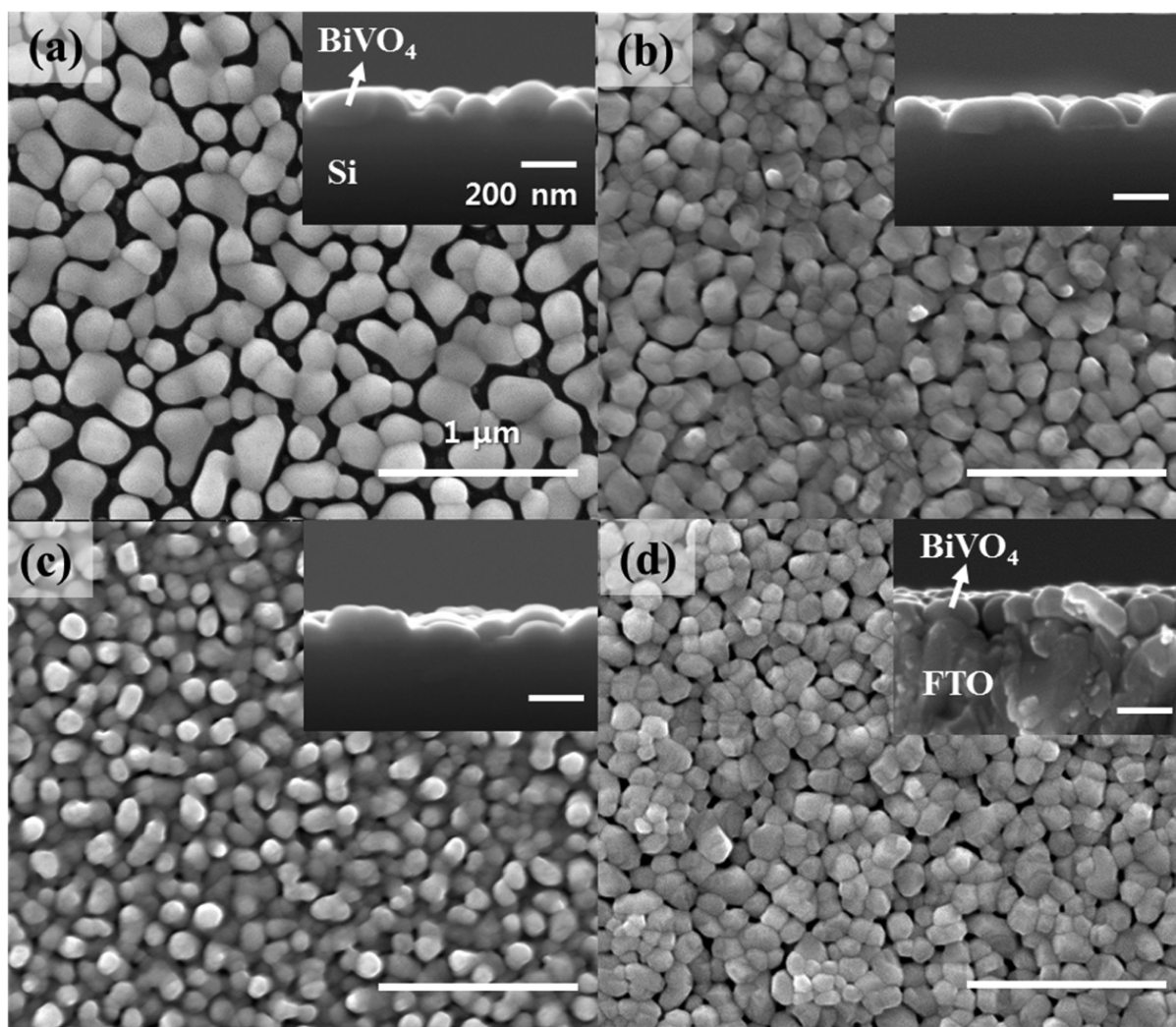
Figure 1. SEM images of (a) Si/BiVO$_4$, (b) Si/TiO$_2$(105)/BiVO$_4$, (c) Si/TiO$_2$(525)/BiVO$_4$, and (d) FTO/BiVO$_4$. The numbers in parentheses indicate the number of layers of TiO$_2$ deposited by ALD. Insets show the corresponding cross-sectional images, showing the average thickness of the BiVO$_4$ layer to be 150−200 nm.

a potentiostat (Ivium Technologies) in a 0.1 M potassium phosphate aqueous electrolyte (pH 7.0), employing a three-electrode configuration with a photoanode working electrode, a Pt counter electrode, and a Ag/AgCl reference electrode. For the ohmic contact with Si substrate-based photoanodes (i.e., Si, Si/BiVO$_4$, and Si/TiO$_2$/BiVO$_4$ photoanodes), the back side of the Si wafer was scratched, and an In/Ga eutectic alloy (Sigma-Aldrich) was added. Then, Cu wire was connected to the back side of the Si substrate by using a silver paste, and electrical insulating epoxy sealed the contact. The electrode areas were controlled to have 0.2−0.5 cm^2.

Photoanodic performances of the samples were measured by linear sweep voltammetry, which was scanned from the cathodic to anodic potential direction with a scan rate of 10 mV s^{-1}. All measured potential values were converted relative to RHE using E (vs RHE) = E (vs Ag/AgCl) + 0.209 + 0.059 V × pH. Simulated solar light was produced by a solar simulator (ABET, Sun 2000) equipped with a 300 W Xe lamp and air mass (AM) 1.5 filter, and the input power intensity (1 sun condition = 100 mW cm^{-2}) was confirmed by a reference silicon solar cell. To investigate the PEC performance of the sample photoanodes without the effect of water oxidation kinetics, 1.0 M Na$_2$SO$_3$ was added to the electrolyte to introduce hole scavengers.

The incident photon-to-electron conversion efficiency (IPCE) was measured at 1.23 V versus RHE. A water IR filter equipped with a 1000 W Xe lamp (Newport) was coupled with a motorized monochromator (Newport, Cornerstone 130) to monitor the incident light, whose intensity at each wavelength was measured with a calibrated Si photodiode. The IPCE was calculated using the following equation

$$\text{IPCE (\%)} = \frac{I_{ph}\ (\text{mA cm}^{-2}) \times 1239.8\ (\text{V nm})}{P_{mono}\ (\text{mW cm}^{-2}) \times \lambda\ (\text{nm})} \times 100 \tag{1}$$

where I_{ph} is the measured photocurrent density, λ is the wavelength of the incident light, and P_{mono} is the power intensity of the incident light at each wavelength. The measured IPCE data were validated by comparing the integrated photocurrent based on the IPCE data with the photocurrent under the simulated sunlight condition, which matched with <5% deviation.

2.3. Characterizations. Top-view and cross-sectional images of FTO/BiVO$_4$, Si/BiVO$_4$, and Si/TiO$_2$/BiVO$_4$ were taken by scanning electron microscopy (SEM) (FEI, Inspect F50), and transmission electron microscopy (TEM) (FEI, Technai) was used to characterize the thickness and crystal structure of the TiO$_2$ layer. UV−vis spectrometry (Varian, Cary 100) was employed to analyze the absorbance of FTO/BiVO$_4$ and FTO/TiO$_2$/BiVO$_4$. X-ray diffraction (XRD) (Bruker Advance GADDs) was used to characterize the crystal structure of Si/BiVO$_4$ and Si/TiO$_2$/BiVO$_4$.

3. RESULTS AND DISCUSSION

The SEM images of the heterojunction films showed the nanostructure of the $BiVO_4$ layer on bare Si substrate (Figure 1a). The bright and dark regions in Figure 1a indicate the deposition of $BiVO_4$ and bare Si surface (no or little deposition of $BiVO_4$), respectively. The thickness of the $BiVO_4$ film was approximately 150–200 nm on average, according to the cross-sectional SEM image, but some parts were thinner than 50 nm. If bare Si is exposed to an aqueous electrolyte, Si is easily oxidized under an anodic potential prior to the oxidation of the water, and the resulting silicon oxide layer can prohibit efficient charge transfer between Si and $BiVO_4$ or Si and the electrolyte. We observed a fast decrease in the photoanodic current and oxidation of Si when $BiVO_4$ was applied directly to a bare Si substrate (Figure S1 of the Supporting Information), which could be caused by the penetration of the electrolyte through the porous $BiVO_4$ layer. To protect the bottom layer of Si, therefore, a thin film of TiO_2 was introduced by ALD onto the Si substrate, followed by $BiVO_4$ deposition. Thin films of ALD TiO_2 have been applied previously to protect the bottom of unstable photoelectrode materials from corrosion in PEC water splitting applications.[19,28,29]

The morphologies and photoanodic activities of the heterojunction photoanodes were studied by changing the thickness of the TiO_2 film, controlled by the number of ALD cycles (35, 105, 525, or 1050). When 35 cycles of ALD TiO_2 were deposited on the Si substrate [$Si/TiO_2(35)$], the morphology of the $BiVO_4$ film [$Si/TiO_2(35)/BiVO_4$] was not significantly changed compared to that of $Si/BiVO_4$ (Figure 1a). When the number of ALD cycles increased to 105 and beyond, compact $BiVO_4$ films (Figure 1b,c) were obtained. Lastly, Figure 1d shows the $BiVO_4$ films coated on the FTO substrate ($FTO/BiVO_4$). Although small variations in the morphology of the porous $BiVO_4$ film on the various substrates were observed in the top-down SEM images, the cross-sectional SEM images confirmed that the average thickness of the spin-coated $BiVO_4$ layer remained within the range of 150–200 nm, regardless of the types of the bottom substrates.

Material characterization was further conducted by collecting XRD patterns, which showed that all of the deposited $BiVO_4$ films on Si or Si/TiO_2 substrates had a monoclinic crystal structure (Figure 2), the same as that coated on the FTO substrate.[27] Most of the XRD intensity peaks were assigned to $BiVO_4$, and the Si peaks from the bottom substrate either overlapped with $BiVO_4$ peaks or were too small to be distinguished from them. The only difference between the XRD analysis of the $Si/BiVO_4$ and $Si/TiO_2/BiVO_4$ samples was the evolution of a small peak at $2\theta = 25.35°$, which was observed when the number of ALD TiO_2 cycles exceeded 525 (Figure 2e,f). This peak is associated with the (101) plane of TiO_2's anatase structure, the strongest major peak from powder diffraction. TiO_2 films thinner than those produced by 525 ALD cycles did not show any crystalline TiO_2 patterns in XRD analysis, meaning that the films were either amorphous or too thin to be detected by XRD. XRD patterns of the as-prepared Si/TiO_2 films without $BiVO_4$ layer deposition were also measured (Figure S2 of the Supporting Information), and the same peak at $2\theta = 25.35°$ was obtained with only $Si/TiO_2(525)$ and $Si/TiO_2(1050)$.

To further characterize the crystal structure and the interface of $Si/TiO_2/BiVO_4$ heterojunction, high-resolution transmission electron microscope (HRTEM) images were taken (Figure 3).
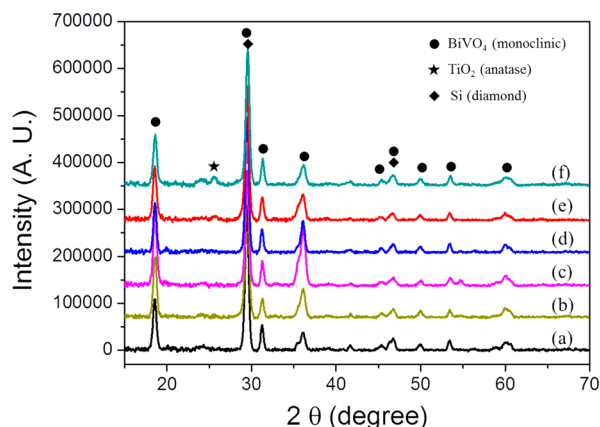

Figure 2. X-ray diffraction patterns of (a) $Si/BiVO_4$, (b) $Si/TiO_2(35)/BiVO_4$, (c) $Si/TiO_2(105)/BiVO_4$, (d) $Si/TiO_2(245)/BiVO_4$, (e) $Si/TiO_2(525)/BiVO_4$, and (f) $Si/TiO_2(1050)/BiVO_4$, showing the observation of the TiO_2 anatase (101) peak when the number of ALD cycles (indicated in parentheses) was larger than 525.

HRTEM imaging revealed that all of the ALD TiO_2 layers had polycrystalline structures for $Si/TiO_2(35)/BiVO_4$, $Si/TiO_2(105)/BiVO_4$, and $Si/TiO_2(525)/BiVO_4$, and their longest d spacing was 3.52 Å, which matches with that of anatase TiO_2 (101) planes. The average film thickness of ALD TiO_2 was 4–5 nm for 35 cycles, 8–9 nm for 105 cycles, and 20–25 nm for 525 cycles, showing a growth rate of 0.4–0.45 Å/cycle. Lattice fringes from the Si and $BiVO_4$ layers also confirmed the diamond structure of Si and monoclinic structure of $BiVO_4$, consistent with the XRD patterns shown in Figure 2. The $BiVO_4$ layer covered the crystalline TiO_2 film well without any observable extra interlayers, while a thin amorphous layer of ~2 nm was observed between Si and TiO_2. The amorphous layer was associated with native silicon oxide (SiO_2) and/or partially mixed oxides of Si and Ti. ALD TiO_2 was deposited on the bare Si (100) substrate without etching of the native silicon oxide layer, which has a typical thickness of 1.2–3.0 nm, to aid in the conformal and pinhole-free deposition of TiO_2. This thin amorphous layer may reduce the lattice mismatch strain between the crystalline Si and TiO_2, and it was found to be thin enough to permit facile electron tunneling in the photoanodic application.[29]

To examine the photoanodic properties of the $Si/BiVO_4$ heterojunction films and the influence of the thickness of the TiO_2 protecting layer on the photocatalytic activities of the films, linear sweep voltammetry (LSV) (Figure 4a) and photocurrent densities at 1.23 V versus RHE (Figure 4b) of the heterojunction films were compared with those of the $FTO/BiVO_4$ electrode under sunlight-simulated conditions. Enhanced photoanodic activities were obtained with samples in which the ALD TiO_2 layer had been deposited for more than 105 cycles, and the highest photocurrent density improvement was achieved with 525 cycles of ALD TiO_2. The enhancement in the photocurrent density was outstanding when the applied potential was low (specifically in the region of 0.4–1.0 V vs RHE), and thus, the decrease in the onset potential of the photocurrent was obviously observed.

Generally, when the applied potential is close to the flat band potential of the semiconductor electrode, the decreased level of band bending at the semiconductor/electrolyte interface exacerbates recombination loss, and the photocurrent drops to zero with the loss of the driving force to separate
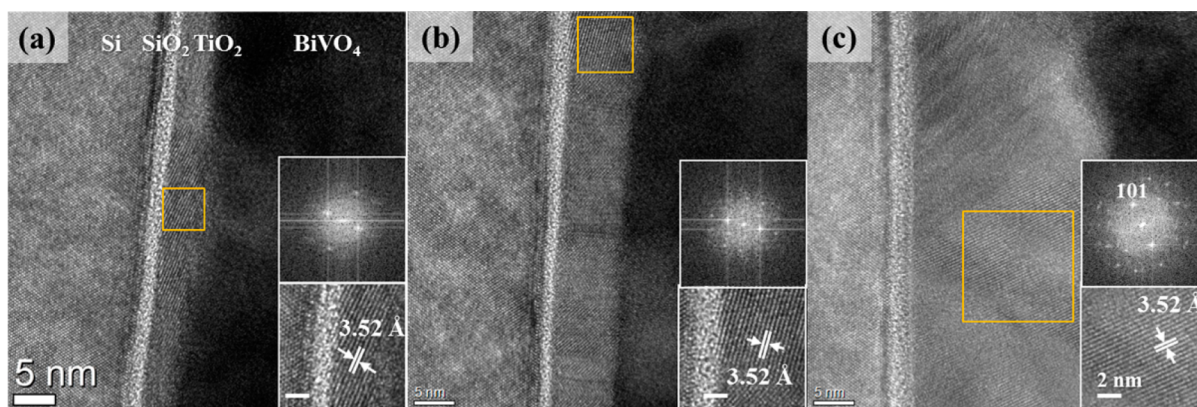
Figure 3. HRTEM images of (a) $Si/TiO_2(105)/BiVO_4$, (b) $Si/TiO_2(245)/BiVO_4$, and (c) $Si/TiO_2(525)/BiVO_4$, showing the interfacial TiO_2 ALD layer. The insets are the magnified images and FFT patterns of the selected areas, indicating the crystal structure of the anatase TiO_2 interlayer.
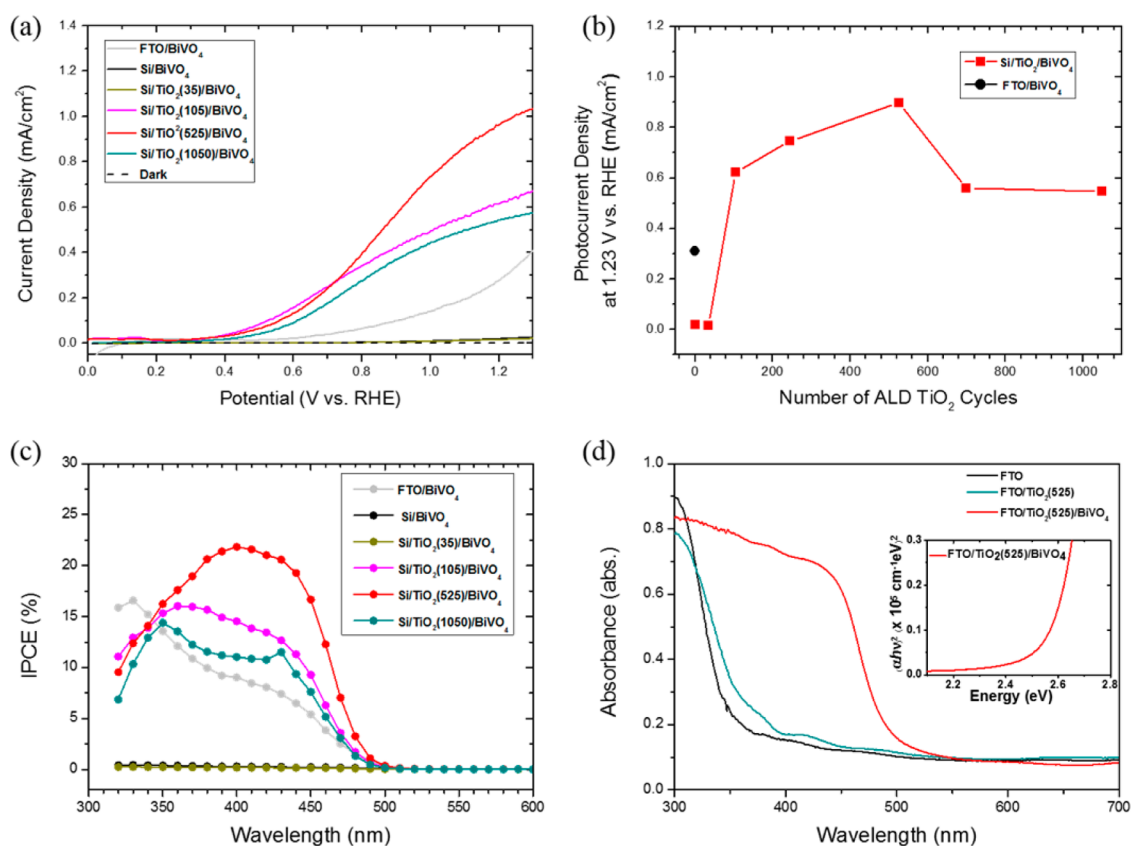

Figure 4. (a) LSV of various photoanodes measured in a phosphate buffer solution under simulated sunlight (100 mW/cm²). (b) Dependence of photocurrent density on the number of ALD TiO_2 cycles. (c) IPCE of various photoanodes. (d) UV−vis absorption spectra of FTO, FTO/TiO_2, and $TiO_2/BiVO_4$ film showing $BiVO_4$ is a visible light absorber with an E_g of 2.5 eV.

photogenerated charges in the photoanodic electrode. Therefore, the enhanced photocurrent density and lowered onset potential observed with the $Si/TiO_2/BiVO_4$ films are consistent with the idea that charge separation in the $BiVO_4$ layer is improved by the addition of the heterojunction, as suggested in Scheme 1a. Recombination between the photogenerated electrons in $BiVO_4$ and holes in Si results in charge separation of residual electrons and holes in the Si and $BiVO_4$ layers, respectively. Such charge separation is desirable for overall water splitting, in which water oxidation occurs on the $BiVO_4$ surface and hydrogen generation occurs on the counter electrode. The electrons in the Si CB can have higher

energetics to reduce hydrogen at the Pt counter electrode because the more negative CB potential of Si compared to that of $BiVO_4$ results in a cathodical shift of onset potential for water oxidation with $Si/TiO_2/BiVO_4$ heterojunction films.

In contrast, the photocurrent densities of $Si/BiVO_4$ and $Si/TiO_2(35)/BiVO_4$ heterojunction films were much lower than that of $FTO/BiVO_4$. This is because the porous nature of $BiVO_4$ layer cannot protect the bottom Si layer from oxidation, which causes poor heterojunction formation and a significant decrease in the photocurrent density. This result indicates that a certain thickness of an ALD TiO_2 film is critical for taking
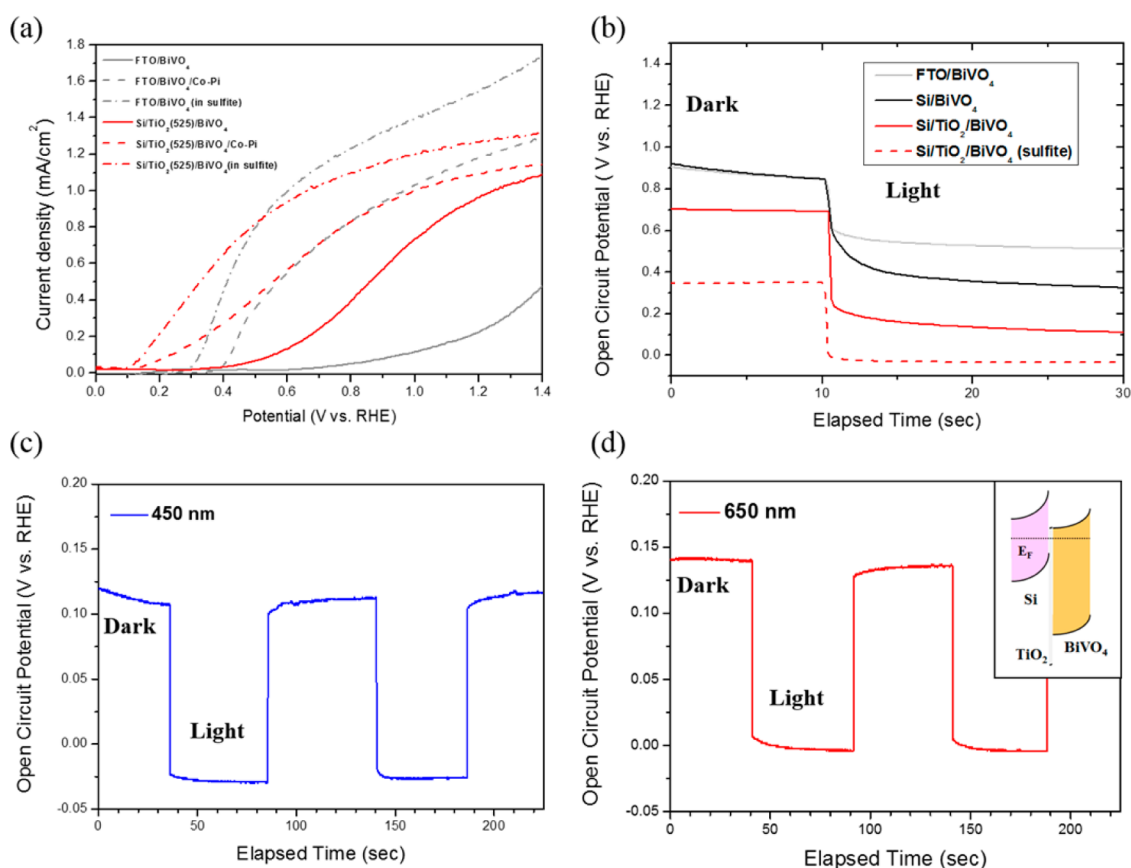
Figure 5. (a) Photocurrent density of FTO/BiVO$_4$ and Si/TiO$_2$(525)/BiVO$_4$ photoanodes with and without Co-Pi deposition in a phosphate-buffered electrolyte (pH 7.0), except the dashed red line for Si/TiO$_2$(525)/BiVO$_4$ was measured in 1.0 M Na$_2$SO$_3$/phosphate-buffered electrolyte. (b) Open circuit potentials of photoanodes measured in darkness and under simulated sunlight and open circuit potentials of Si/TiO$_2$/BiVO$_4$ measured under (c) $\lambda = 450$ nm and (d) $\lambda = 650$ nm. The inset in panel d is a schematic diagram showing the band bending of Si and BiVO$_4$.

advantage of the heterojunction effect probably because of the instability of the Si surface for anodic use in PEC cells.

The photocurrent dependence on the thickness of ALD TiO$_2$ shows that there are optimal ranges of ALD TiO$_2$ cycles (Figure 4b). The highest photocurrent density at 1.23 V versus RHE was obtained with 525 cycles, where more than 3 times the photocurrent enhancement was achieved compared to that of the FTO/BiVO$_4$ film. It is expected that a thick layer of TiO$_2$ would be harmful to the series conductivity of the anode film because of the poor electrical conductivity of TiO$_2$, and it can also compete for light absorption with the BiVO$_4$ layer in the UV region. Therefore, it is reasonable that an optimal thickness of the TiO$_2$ layer was observed.

IPCE measurement showed substantial improvements in the quantum efficiency in the visible region where BiVO$_4$ absorbs (Figure 4c). The IPCE values were almost zero where the incident wavelength (λ) was longer than 530 nm for all photoanodes. The improvement in the visible region ($\lambda < 500$ nm) confirmed that the heterojunction contributes to the charge separation in the BiVO$_4$ layer, resulting in the increased photocurrent density as the suggested charge flows in Scheme 1a. Meanwhile, the IPCE value rather decreased in the UV region with Si/TiO$_2$/BiVO$_4$, probably because the light absorption of BiVO$_4$ competes with that of Si or TiO$_2$. In a dual-absorber system, both BiVO$_4$ and Si should be excited to complete the charge flows and increase the charge separation efficiency. However, the upper BiVO$_4$ layers would absorb strongly in the UV region, and the photons are less likely to

excite Si, which can cause decrease in IPCE under UV irradiation.[21] A decrease in IPCE under regions of shorter wavelength was also observed when the electron transport in the photoanode was poor.[30] The interlayer TiO$_2$ film can increase the series resistance within the Si/TiO$_2$/BiVO$_4$ heterojunction, which may also contribute to the loss of the quantum efficiency in short-wavelength regions.

The IPCE results were compared with the UV–vis absorbance spectra of TiO$_2$/BiVO$_4$ films. The UV–vis absorbance of Si/TiO$_2$/BiVO$_4$ could not be measured because the 500 μm thick Si substrate was too thick and opaque. Instead, we measured the UV–vis absorbance of TiO$_2$(525)/BiVO$_4$ on the transparent FTO substrate (Figure 4d), which showed that the absorption edge ($\lambda = 530$ nm) of the prepared BiVO$_4$ layer was well matched with the tail of the IPCE measurement. In addition, an IPCE value of zero for $\lambda > 530$ nm implies that the light absorption solely by Si cannot contribute to the photo-oxidation current of Si/TiO$_2$/BiVO$_4$ photoanodes, and absorption by Si ($E_g = 1.1$ eV) in the long-wavelength region cannot be utilized for the photoanodic water oxidation reaction because of thermodynamically forbidden hole transfer from Si to BiVO$_4$. The VB edge of the Si is located at a potential more positive than that of TiO$_2$ or that of BiVO$_4$, which blocks the thermodynamic flow of the holes. IPCE values approaching zero in this range confirmed that the charge carriers flowing in the Si/TiO$_2$/BiVO$_4$ junction were different from those in other heterojunctions such as WO$_3$/BiVO$_4$, TiO$_2$/BiVO$_4$, and ZnO/BiVO$_4$, where it was suggested that the

holes were transferred from the bottom metal oxide layer to the top $BiVO_4$ layer, and electrons were transferred in the opposite direction. In short, the light absorption by the bottom Si substrate contributes to the cathodic shift of the onset potential and enhanced charge separation in $BiVO_4$.

Next, OER catalysts were deposited on the $BiVO_4$ surface, and sulfite oxidation was performed with the $Si/TiO_2(525)/BiVO_4$ photoanode to reduce the hole transfer loss across the electrolyte (Figure 5a) to examine the PEC properties further. The photocurrent density and its onset potential can be significantly influenced by poor catalytic kinetics on the $BiVO_4$ surface. Sulfite oxidation with the heterojunction film showed that the photocurrent density was substantially improved and the onset potential of the photocurrent was decreased to as low as 0.1 V versus RHE because of the fast oxidation kinetics. Similarly, a low onset potential was obtained with the $Si/TiO_2/BiVO_4$ photoanode after Co-Pi OER decoration, although the photocurrent density was lower than that during sulfite oxidation. The lower photocurrent density was attributed to the overpotential of Co-Pi OER on the $BiVO_4$ layer for water oxidation, and the photocurrent density may improve further with the development of excellent OER catalysts.

The measured onset potential (0.1 V vs RHE) of the $Si/TiO_2/BiVO_4/Co-Pi$ photoanode was almost 300 mV more cathodic than that of the $FTO/BiVO_4$ photoanode with Co-Pi OER catalysts in our study, showing that a similar amount of cathodic shift was obtained both with and without Co-Pi decoration. However, the enhancement of the photocurrent with the $Si/TiO_2/BiVO_4$ film was not significant in the high-bias potential region after Co-Pi deposition. In the case of Co-Pi-deposited photoanodes, Co-Pi can facilitate hole transfer from the $BiVO_4$ surface to the electrolyte by reducing the required overpotential for water oxidation, and removal of holes from the $BiVO_4$ layer can increase the charge separation efficiency, as well. Therefore, a Co-Pi-deposited heterojunction film would give only less enhancement of charge separation efficiency compared to the photoanodes without Co-Pi OER because Co-Pi already contributes to charge separation in $BiVO_4$ beyond the heterojunction. In addition, the steepness difference in $I-V$ curves may come from the large series resistance of the $Si/TiO_2/BiVO_4$ photoanode probably because of the poor electrical conductivity of interface TiO_2 thin film. For a similar reason, the photocurrent density in the sulfite oxidation electrolyte showed a less steep current increase with the $Si/TiO_2/BiVO_4$ photoanode under high anodic potential, while the onset potential of the photocurrents was more cathodic.

To support the suggested charge separation mechanism within the heterojunction films, open circuit potentials (V_{oc}) were measured both in darkness and under illumination to examine the band bending direction of Si and $BiVO_4$, respectively (Figure 5b−d). V_{oc} of the $FTO/BiVO_4$ (0.51 V vs RHE), $Si/BiVO_4$ (0.33 V vs RHE), and $Si/TiO_2(525)/BiVO_4$ (0.11 V vs RHE) photoanodes commonly showed a cathodic shift under 1 Sun condition compared to that in dark, which displays downward band bending due to Schottky barrier formation at the interface between the semiconductor and the electrolyte. The more cathodic value of V_{oc} for $Si/TiO_2/BiVO_4$ under illumination compared to that of $FTO/BiVO_4$ is consistent with LSV measurement results showing lower onset potentials of the heterojunction films.

In addition, the changes in V_{oc} with the $Si/TiO_2(525)/BiVO_4$ film were monitored in the dark and under illumination

with monochromatic incident light at both $\lambda = 450$ nm (Figure 5c) and 650 nm (Figure 5d). Both Si and $BiVO_4$ can absorb light at $\lambda = 450$ nm, while only Si can be excited at $\lambda = 650$ nm because of its smaller band gap. Figure 5d clearly shows that the V_{oc} also shifted cathodically when only Si was excited by the incident light at $\lambda = 650$ nm. This cathodic V_{oc} shift implies that the Fermi level of Si moves upward under illumination and thus implies the band bending at the Si side is downward in darkness, as shown in the inset of Figure 5d. This Schottky barrier formation in $Si/TiO_2/BiVO_4$ can assist hole transfer from Si to $BiVO_4$ and electron transfer from $BiVO_4$ to Si for the charge recombination at the interface, considering TiO_2 as a thin tunneling layer (see Scheme 1a). It is also possible that high-energy electrons in the CB of $BiVO_4$ are transported to TiO_2 and finally reach the Si layer.[31,32] As shown in Scheme 1a, the suggested charge flow can help charge separation within $BiVO_4$ for the enhancement of photocurrent density and the shift of onset potential with a higher potential of electrons in the conduction band of Si.

Lastly, the two-electrode measurement (Figure S3 of the Supporting Information) was performed with the best performing photoanode. A $Si/TiO_2(525)/BiVO_4/Co-Pi$ photoanode was a working electrode, and a Pt counter electrode was used. In the two-electrode configuration, the onset potential of photocurrents was measured as 0.1 V versus Pt, which was a smaller bias potential compared to the onset potential of the $WO_3/BiVO_4$ heterojunction, reported to have a 0.5 V versus Pt onset potential in the previous study.[15] Moreover, 0.37% of solar-to-hydrogen efficiency was obtained when 0.65 V was applied versus a Pt counter electrode.

The suggested n/n junctions successfully demonstrated the cathodic shift of the photocurrent onset voltage, as well as enhanced charge separation for feasible overall water splitting, although the photocurrent density must be improved further. The photocurrent density is expected to be improved by optimizing the morphology of the heterojunction film, developing $BiVO_4$ or interface TiO_2 deposition condition, OER catalyst development, etc. In addition, this study also represents the importance of the TiO_2 interlayer for the direct combination of $BiVO_4$ on the Si surface, which can be applicable to the Si solar cell/$BiVO_4$ PEC hybrid system.

4. CONCLUSIONS

$Si/TiO_2/BiVO_4$ heterojunction photoanodes were prepared to improve the charge separation in the $BiVO_4$ layer and shift the onset potential of the photocurrent in the cathodic potential direction for water oxidation applications. The thickness of an interlayer ALD TiO_2 thin film was optimized to protect Si from oxidation and to help charge recombination between Si and $BiVO_4$. With the assistance of the charge separation in the heterojunction films, $Si/TiO_2/BiVO_4$ photoanodes showed 3.3-fold enhanced photocurrent density at 1.23 V versus RHE. In addition, its onset potential for the photocurrent shifted negatively by 300 mV compared to that of the $FTO/BiVO_4$ photoanode. Further enhancement of the photoanode activities can be expected via improvement of the interlayer conditions as well as developing cocatalysts. This study suggests that heterojunctions of Si and $BiVO_4$ can reduce the necessary applied potential for efficient overall solar water splitting.

■ ASSOCIATED CONTENT

Ⓢ Supporting Information

Chrono-amperometry of Si/BiVO$_4$ photoanode, XRD patterns of ALD TiO$_2$ thin films on Si substrates, and two electrode measurement results are included in the Supporting Information. This material is available free of charge via the Internet at http://pubs.acs.org.

■ AUTHOR INFORMATION

Corresponding Author

*E-mail: yjhwang@kist.re.kr. Phone: +82-2-958-5227. Fax: +82-2-958-5809.

Author Contributions

H.J. and S.Y.C. contributed equally to this work.

Notes

The authors declare no competing financial interest.

■ ACKNOWLEDGMENTS

■ REFERENCES

(1) Hisatomi, T.; Kubota, J.; Domen, K. Recent Advances in Semiconductors for Photocatalytic and Photoelectrochemical Water Splitting. *Chem. Soc. Rev.* **2014**, *43*, 7520–7535.

(2) Osterloh, F. E. Inorganic Nanostructures for Photoelectrochemical and Photocatalytic Water Splitting. *Chem. Soc. Rev.* **2013**, *42*, 2294–2320.

(3) Dotan, H.; Mathews, N.; Hisatomi, T.; Grätzel, M.; Rothschild, A. On the Solar to Hydrogen Conversion Efficiency of Photoelectrodes for Water Splitting. *J. Phys. Chem. Lett.* **2014**, *5*, 3330–3334.

(4) Khan, S. U. M.; Al-Shahry, M.; Ingler, W. B. Efficient Photochemical Water Splitting by a Chemically Modified n-TiO$_2$. *Science* **2002**, *297*, 2243–2245.

(5) Kalanur, S. S.; Hwang, Y. J.; Chae, S. Y.; Joo, O. S. Facile Growth of Aligned WO$_3$ Nanorods on FTO Substrate for Enhanced Photoanodic Water Oxidation Activity. *J. Mater. Chem. A* **2013**, *1*, 3479–3488.

(6) Sivula, K.; Le Formal, F.; Grätzel, M. Solar Water Splitting: Progress Using Hematite(α-Fe$_2$O$_3$) Photoelectrodes. *ChemSusChem* **2011**, *4*, 432–449.

(7) Kim, T. W.; Choi, K.-S. Nanoporous BiVO$_4$ Photoanodes with Dual-Layer Oxygen Evolution Catalysts for Solar Water Splitting. *Science* **2014**, *343*, 990–994.

(8) Yokoyama, D.; Hashiguchi, H.; Maeda, K.; Minegishi, T.; Takata, T.; Abe, R.; Kubota, J.; Domen, K. Ta$_3$N$_5$ Photoanodes for Water Splitting Prepared by Sputtering. *Thin Solid Films* **2011**, *519*, 2087–2092.

(9) Xu, Y.; Zhao, W. W.; Xu, R.; Shi, Y. M.; Zhang, B. Synthesis of Ultrathin CdS Nanosheets as Efficient Visible-Light-Driven Water Splitting Photocatalysts for Hydrogen Evolution. *Chem. Commun.* **2013**, *49*, 9803–9805.

(10) Park, Y.; McDonald, K. J.; Choi, K.-S. Progress in Bismuth Vanadate Photoanodes for Use in Solar Water Oxidation. *Chem. Soc. Rev.* **2013**, *42*, 2321–2337.

(11) Abdi, F. F.; Han, L.; Smets, A. H. M.; Zeman, M.; Dam, B.; van de Krol, R. Efficient Solar Water Splitting by Enhanced Charge Separation in a Bismuth Vanadate-Silicon Tandem Photoelectrode. *Nat. Commun.* **2013**, *4*, No. 2195.

(12) Ding, C. M.; Qin, W.; Wang, N.; Liu, G. J.; Wang, Z. L.; Yan, P. L.; Shi, J. Y.; Li, C. Solar-to-Hydrogen Efficiency Exceeding 2.5% Achieved for Overall Water Splitting with an All Earth-Abundant Dual-Photoelectrode. *Phys. Chem. Chem. Phys.* **2014**, *16*, 15608–15614.

(13) Ng, Y. H.; Iwase, A.; Kudo, A.; Amal, R. Reducing Graphene Oxide on a Visible-Light BiVO$_4$ Photocatalyst for an Enhanced Photoelectrochemical Water Splitting. *J. Phys. Chem. Lett.* **2010**, *1*, 2607–2612.

(14) Zhou, M.; Bao, J.; Xu, Y.; Zhang, J. J.; Xie, J. F.; Guan, M. L.; Wang, C. L.; Wen, L. Y.; Lei, Y.; Xie, Y. Photoelectrodes Based Upon Mo:BiVO$_4$ Inverse Opals for Photoelectrochemical Water Splitting. *ACS Nano* **2014**, *8*, 7088–7098.

(15) Chae, S. Y.; Jung, H.; Jeon, H. S.; Min, B. K.; Hwang, Y. J.; Joo, O. S. Morphology Control of One-Dimensional Heterojunctions for Highly Efficient Photoanodes Used for Solar Water Splitting. *J. Mater. Chem. A* **2014**, *2*, 11408–11416.

(16) Rao, P. M.; Cai, L. L.; Liu, C.; Cho, I. S.; Lee, C. H.; Weisse, J. M.; Yang, P. D.; Zheng, X. L. Simultaneously Efficient Light Absorption and Charge Separation in WO$_3$/BiVO$_4$ Core/Shell Nanowire Photoanode for Photoelectrochemical Water Oxidation. *Nano Lett.* **2014**, *14*, 1099–1105.

(17) Abdi, F. F.; van de Krol, R. Nature and Light Dependence of Bulk Recombination in Co-Pi-Catalyzed BiVO$_4$ Photoanodes. *J. Phys. Chem. C* **2012**, *116*, 9398–9404.

(18) Seabold, J. A.; Choi, K. S. Efficient and Stable Photo-Oxidation of Water by a Bismuth Vanadate Photoanode Coupled with an Iron Oxyhydroxide Oxygen Evolution Catalyst. *J. Am. Chem. Soc.* **2012**, *134*, 2186–2192.

(19) Hwang, Y. J.; Boukai, A.; Yang, P. D. High Density n-Si/n-TiO$_2$ Core/Shell Nanowire Arrays with Enhanced Photoactivity. *Nano Lett.* **2009**, *9*, 410–415.

(20) Mayer, M. T.; Du, C.; Wang, D. Hematite/Si Nanowire Dual-Absorber System for Photoelectrochemical Water Splitting at Low Applied Potentials. *J. Am. Chem. Soc.* **2012**, *134*, 12406–12409.

(21) Qi, X. P.; She, G. W.; Huang, X.; Zhang, T. P.; Wang, H. M.; Mu, L. X.; Shi, W. S. High-Performance n-Si/α-Fe$_2$O$_3$ Core/Shell Nanowire Array Photoanode Towards Photoelectrochemical Water Splitting. *Nanoscale* **2014**, *6*, 3182–3189.

(22) Hu, S.; Shaner, M. R.; Beardslee, J. A.; Lichterman, M.; Brunschwig, B. S.; Lewis, N. S. Amorphous TiO$_2$ Coatings Stabilize Si, Gaas, and Gap Photoanodes for Efficient Water Oxidation. *Science* **2014**, *344*, 1005–1009.

(23) Su, J. Z.; Guo, L. J.; Bao, N. Z.; Grimes, C. A. Nanostructured WO$_3$/BiVO$_4$ Heterojunction Films for Efficient Photoelectrochemical Water Splitting. *Nano Lett.* **2011**, *11*, 1928–1933.

(24) Hong, S. J.; Lee, S.; Jang, J. S.; Lee, J. S. Heterojunction BiVO$_4$/WO$_3$ Electrodes for Enhanced Photoactivity of Water Oxidation. *Energy Environ. Sci.* **2011**, *4*, 1781–1787.

(25) Zhang, L. W.; Reisner, E.; Baumberg, J. J. Al-Doped ZnO Inverse Opal Networks as Efficient Electron Collectors in BiVO$_4$ Photoanodes for Solar Water Oxidation. *Energy Environ. Sci.* **2014**, *7*, 1402–1408.

(26) Ho-Kimura, S.; Moniz, S. J. A.; Handoko, A. D.; Tang, J. W. Enhanced Photoelectrochemical Water Splitting by Nanostructured BiVO$_4$-TiO$_2$ Composite Electrodes. *J. Mater. Chem. A* **2014**, *2*, 3948–3953.

(27) Zhong, D. K.; Choi, S.; Gamelin, D. R. Near-Complete Suppression of Surface Recombination in Solar Photoelectrolysis by "Co-Pi" Catalyst-Modified W:BiVO$_4$. *J. Am. Chem. Soc.* **2011**, *133*, 18370–18377.

(28) Paracchino, A.; Laporte, V.; Sivula, K.; Grätzel, M.; Thimsen, E. Highly Active Oxide Photocathode for Photoelectrochemical Water Reduction. *Nat. Mater.* **2011**, *10*, 456–461.

(29) Chen, Y. W.; Prange, J. D.; Dühnen, S.; Park, Y.; Gunji, M.; Chidsey, C. E. D.; McIntyre, P. C. Atomic Layer-Deposited Tunnel Oxide Stabilizes Silicon Photoanodes for Water Oxidation. *Nat. Mater.* **2011**, *10*, 539–544.

(30) Popkirov, G.; Schindler, R. M. Spectral Dependence of the Quantum Efficiency of Thin Film Semiconductor Photoelectrodes. *Sol. Energy Mater.* **1986**, *13*, 161−174.

(31) Fu, X. D.; Xie, M. Z.; Luan, P.; Jing, L. Q. Effective Visible-Excited Charge Separation in Silicate-Bridged $ZnO/BiVO_4$ Nanocomposite and Its Contribution to Enhanced Photocatalytic Activity. *ACS Appl. Mater. Interfaces* **2014**, *6*, 18550−18557.

(32) Xie, M. Z.; Fu, X. D.; Jing, L. Q.; Luan, P.; Feng, Y. J.; Fu, H. G. Long-Lived, Visible-Light-Excited Charge Carriers of $TiO_2/BiVO_4$ Nanocomposites and Their Unexpected Photoactivity for Water Splitting. *Adv. Energy Mater.* **2014**, *4*, 1300995.